Optimal Popov Controller Analysis and Synthesis for Systems with Real Parameter Uncertainties

Jonathan P. How, Emmanuel G. Collins, and Wassim M. Haddad

Abstract— **Robust performance analysis plays an important role in the design of controllers for uncertain multivariable systems. Recent research has investigated the use of absolute stability criteria to develop less conservative analysis tests for systems with linear and nonlinear real parameter uncertainties. This note extends previous work on optimal $\mathcal{H}_2$ performance analysis using the Popov criterion by presenting an numerical homotopy algorithm that can be used to analyze systems with less restrictive assumptions on the structure of the uncertainty block. The technique is used to compare relative robustness capabilities of the various control algorithms that have been designed for the Middeck active control experiment (MACE). The analysis is combined with the previously presented Popov controller synthesis to yield compensators that guarantee robust performance for systems with real parameter uncertainty.**

I. Introduction

THE design of high authority, robust controllers for multi-input multioutput (MIMO) systems with uncertain dynamics can be very complicated and often requires several iterations of the synthesis procedure. The difficulties in this process have been clearly demonstrated during the development of the Middeck active control experiment (MACE), which is a space shuttle experiment flown on STS-67 in March, 1995, to investigate the extent to which the on-orbit behavior of a precision-controlled spacecraft can be predicted and controlled using analysis and ground testing [1]. Recent work in this program has focused on control design using the dynamics predicted by the finite element model (FEM) [1], [2]. Due to errors in the predictions of these models, good analysis and synthesis techniques that can guarantee robust performance are required.

An important part of the coherent control design methodology that has been developed for MACE are the analysis tools used to assess stability (multivariable Nyquist or Nichols), sensitivity (singular values of the return difference), and robust performance (evaluation on data and model). These analysis tools, however, are not effective for systems with real parameter uncertainty, such as modal frequency errors. Thus, work has also concentrated on developing less conservative analysis tests for systems with this type of uncertainty. The Popov analysis and synthesis algorithms have been developed from research on the Popov stability criterion [3] from the absolute stability theory [4]–[6].

The primary purpose of this note is to present several advances in Popov controller analysis and synthesis. Examples in [7] illustrate that the state-space Popov analysis criterion is much less conservative than similar positive real and small gain ($\mathcal{H}_\infty$) criteria. This paper extends these previous results by considering systems with multiple uncertainties that have both upper and lower sector-bounds. The stability criterion is also developed using a more general stability multiplier and fewer restrictions on the structure of the system uncertainty. The optimal Popov analysis algorithm is used to compare several robust controllers that were designed using a finite element model of MACE [1], [8]. One of these controllers is then refined using the optimal Popov controller synthesis algorithm developed in [5], [9], and [10]. These combined analysis and synthesis algorithms yield an improved initial condition for the synthesis problem, which is one of the main difficulties with the original synthesis approach [5], [9].

II. Robust Performance Problem

A. Robust Performance Analysis

The basis for the analysis and synthesis approach to robust control design is discussed in detail in [6] and [10]. The objective of the robust performance problem is to develop the worst-case $\mathcal{H}_2$ norm over $\mathcal{U}$ of the expected value of a quadratic in $z(t)$ for the uncertain system

$$\begin{aligned} \dot{x} &= (A + \Delta A)x + B_w w \\ z &= C_z x \end{aligned} \tag{1}$$

where $x \in \mathbb{R}^n$, $A \in \mathbb{R}^{n\times n}$ denotes the nominal dynamics matrix, ΔA denotes a particular perturbation of A belonging to a specified set $\mathcal{U}$, $w(t)$ is an unit intensity white noise signal, and $z(t) \in \mathbb{R}^q$ is a vector of outputs. In particular, the aim is to determine a performance bound β satisfying

$$J(\mathcal{U}) \triangleq \sup_{\Delta A \in \mathcal{U}} \limsup_{t\to\infty} \mathbb{E}\{\|z(t)\|_2^2\} \leq \beta. \tag{2}$$

In the following, we consider a dynamic system with several (m) decoupled, real parameter scalar uncertainties that are modeled as time-invariant sector-bounded nonlinear functions, and develop a stability test using Popov's stability criterion. This test involves a frequency dependent multiplier $W(s) = H + Ns$, $H > 0$, and $N \geq 0$. In this case, the uncertainty

Manuscript received May 9, 1994; revised June 1, 1995. Recommended by Associate Editor, J. M. Maciejowski. This work was supported in part by the NASA In-Step Office under (NAS1-18690), by NASA Headquarters (NAGW-1335) to the MIT Space Engineering Research Center, NSF Grants ECS-9109558 and ECS-9350181, and AFOSR Contract F49620-91-C0019.

J. P. How is with the Department of Aeronautics and Astronautics, Stanford University, Stanford, CA 94305 USA.

E. G. Collins is with the Department of Mechanical Engineering, Florida A&M/Florida State University, Tallahassee, FL 32316 USA.

W. M. Haddad is with the School of Aerospace Engineering, Georgia Institute of Technology, Atlanta, GA 30332–0150 USA.

Publisher Item Identifier S 1063-6536(96)02079-9.

set $\mathcal{U}$ is defined by

$$\mathcal{U} \triangleq \{\Delta A \in \mathbb{R}^{n\times n}: \Delta A = B_0 F C_0,\ M_1 \le F \le M_2\}. \quad (3)$$

The fixed matrices $B_0 \in \mathbb{R}^{n\times m}$ and $C_0 \in \mathbb{R}^{m\times n}$ denote the structure of the uncertainty, and $F \in \mathbb{D}^m$ (the set of $m \times m$ diagonal matrices) is an uncertain diagonal matrix bounded by the diagonal matrices M_1 and M_2. In the following development, the diagonal values of M_1 and M_2 represent the guaranteed limits of robust stability for the closed-loop system.

Theorem 1 [6]: Let $M_1, M_2, N, H \in \mathbb{D}^m$ be such that $M_2 - M_1$ is positive definite, N is nonnegative definite, H is positive definite, and α is a positive scalar. If there exists a nonnegative definite matrix P satisfying

$$\begin{aligned} 0 = &(A - B_0 M_1 C_0)^T P + P(A - B_0 M_1 C_0) \\ &+ [HC_0 + NC_0(A - B_0 M_1 C_0) - B_0^T P]^T R_0^{-1} \\ &\cdot [HC_0 + NC_0(A - B_0 M_1 C_0) - B_0^T P] + \alpha R_{xx} \end{aligned} \quad (4)$$

where

$$R_{xx} \triangleq C_z^T C_z,$$
$$V_{xx} \triangleq B_w B_w^T$$

and

$$\begin{aligned} R_0 \triangleq\ &[H(M_2 - M_1)^{-1} - NC_0 B_0] \\ &+ [H(M_2 - M_1)^{-1} - NC_0 B_0]^T > 0 \end{aligned}$$

then $(A + \Delta A, C_z)$ is detectable, for all $\Delta A \in \mathcal{U}$, if and only if $A + \Delta A$ is asymptotically stable, for all $\Delta A \in \mathcal{U}$. In this case a worst-case overbound of the cost function is given by

$$J(\mathcal{U}) \le \overline{J} \triangleq \frac{1}{\alpha} \operatorname{tr}[P + C_0^T (M_2 - M_1) N C_0] V_{xx}. \quad (5)$$

This theorem provides a means of determining the robust performance of a given control design. That is, for a given $\mathcal{H}_2$ cost functional, the worst-case overbound of the cost functional can be used to approximate the closed-loop performance for given guaranteed stability bounds. Frequency domain sufficient conditions for the existence of a solution to (4) are given in [5] and [7] in terms of off-axis circle criteria.

B. Solution Algorithm

Determining the robust stability and performance bounds using the results in Theorem 1 requires the solution of coupled nonlinear algebraic equations. As discussed in [11], continuation, or homotopy, algorithms are an effective technique for solving problems of this type. The homotopy algorithm from [7] is used in this paper to consider a significantly more complicated system with multiple uncertainties that have both upper and lower sector-bounds. The structure of these uncertainties is also made less restrictive because we do not require that $C_0 B_0 = 0$. This section provides an outline of the homotopy algorithm, and an example of the approach is presented in the last section.

For clarity, the cost in Theorem 1 is rewritten here as

$$\overline{J} = \frac{1}{\alpha} \operatorname{tr}\{[(P + C_0^T (M_2 - M_1) N C_0] V_{xx}\} \quad (6)$$

where P is the solution of

$$\begin{aligned} 0 = &A_m^T P + P A_m \\ &+ (\overline{C} - B_0^T P)^T R_0^{-1} (\overline{C} - B_0^T P) + \alpha R_{xx} \end{aligned} \quad (7)$$

and $A_m \triangleq A - B_0 M_1 C_0$, $\overline{C} \triangleq HC_0 + NC_0 A_m$, $C_{ricc} \triangleq \overline{C} - B_0^T P$, $A_1 \triangleq A_m - B_0 R_0^{-1} \overline{C}$, $A_2 \triangleq A_m - B_0 R_0^{-1} C_{ricc}$. With these definitions, (7) can be rewritten in the more familiar form

$$0 = A_1^T P + P A_1 + \overline{C}^T R_0^{-1} \overline{C} + \alpha R_{xx} + P B_0 R_0^{-1} B_0^T P. \quad (8)$$

The Lagrangian ($\mathcal{L}$) for the system is then formed by combining the cost overbound in (6) with the constraint in (7) using Lagrange multiplier matrix Q. The derivatives of this Lagrangian with respect to the free parameters in the design are the first-order necessary conditions that must be satisfied to determine an optimal solution. In particular, differentiating with respect to P yields a Lyapunov equation for the Lagrange multiplier matrix Q

$$0 = A_2 Q + Q A_2^T + \frac{1}{\alpha} V_{xx}. \quad (9)$$

Note that, if $(\cdot)$ refers to any free parameter in the optimization process, then $\partial\mathcal{L}/\partial(\cdot) = \partial\overline{J}/\partial(\cdot)$. The optimization problem then is to find values of α, H, and N that satisfy

$$\frac{\partial \overline{J}}{\partial \alpha} \triangleq H_1 = \operatorname{tr}[Q R_{xx}] - \frac{1}{\alpha} \overline{J} = 0, \quad (10)$$

$$\begin{aligned} \frac{\partial \overline{J}}{\partial N} \triangleq H_2 = &\frac{1}{\alpha} (M_2 - M_1) C_0 V_{xx} C_0^T \\ &+ 2R_0^{-1} C_{ricc} Q A_2^T C_0^T = 0, \end{aligned} \quad (11)$$

$$\begin{aligned} \frac{\partial \overline{J}}{\partial H} \triangleq H_3 = &2R_0^{-1} C_{ricc} Q \\ &\cdot [C_0 - (M_2 - M_1)^{-1} R_0^{-1} C_{ricc}]^T = 0 \end{aligned} \quad (12)$$

where P and Q are the solutions of (7) and (9), respectively. Note that only the elements of H_2 and H_3 corresponding to free parameters in N and H can be set to zero in the optimization process [5], [12].

The goal is to solve (10)–(12) for several values of M_1 and M_2 to determine: 1) how $\overline{J}$ changes as the sector-bounds increase in magnitude, and 2) the largest magnitudes of the robust bounds for which the system is predicted to remain stable.

C. Continuation Map for Optimal Popov Analysis

There are several steps that must be performed to develop the continuation map for this analysis. The first step is to define a vector η which includes the free elements of the multipliers α, H, and N. Note that in general, not all elements of the multiplier matrices are arbitrary, so we can only optimize with respect to the parameters that are free. Thus, we use a generalized $\operatorname{vec}_N(\cdot)$ operator that extracts the free parameters of a symmetric block diagonal matrix, and assembles them in a column vector. The free elements of the multiplier matrices H and N are then written as

$$\theta \triangleq \begin{bmatrix} \operatorname{vec}_N(N) \\ \operatorname{vec}_H(H) \end{bmatrix}. \quad (13)$$

The symbol θ_j refers to any free element of the multiplier matrices. The vector $\eta \triangleq [\alpha \quad \theta^T]^T$ then contains all of the free parameters in the optimization problem. The results of this paper are developed for the special case of N and H diagonal, and for convenience, it is assumed that the same elements of the multiplier matrices N and H are free.

The next step in the process is to define the homotopy procedure, or continuation map. To begin, consider the upper and lower sector-bounds as functions of a continuation parameter $\lambda \in [0, \quad 1]$, so that $M_1(\lambda) = M_{1o} + \lambda(M_{1f} - M_{1o})$, and $M_2(\lambda) = M_{2o} + \lambda(M_{2f} - M_{2o})$. Note that $M_2(0) = M_{2o}$ and $M_2(1) = M_{2f}$. The overall goal is to solve the optimization problem at $\lambda = 1$. It is often quite difficult, however, to develop valid initial conditions for the optimization at this point. Thus, a starting point which is simpler to initialize is introduced and corresponds to $\lambda = 0$. The purpose of the homotopy procedure is to obtain a solution to the optimization problem at $\lambda = 1$ by starting at $\lambda = 0$ and predicting the solution at $\lambda + \Delta\lambda$ based on the system derivatives and the solution at λ [7].

The continuation map is defined as the gradient of the upper bound on the cost function for the homotopy parameters M_1 and M_2. To compute this map, define

$$L(\eta, \lambda) \triangleq \begin{bmatrix} H_1(\eta, \lambda) \\ \text{vec}_N [H_2(\eta, \lambda)] \\ \text{vec}_N [H_3(\eta, \lambda)] \end{bmatrix}. \tag{14}$$

Then, as indicated by (10)–(12), the continuation curve is given by $L(\eta, \lambda) = 0$ for $\lambda \in [0, \quad 1]$. Taking both α and θ to be functions of λ, we can differentiate $L[\eta(\lambda), \lambda] = 0$ with respect to λ to yield Davidenko's differential equation [13], [14]

$$\frac{\partial L}{\partial \eta} \frac{d\eta}{d\lambda} + \frac{\partial L}{\partial \lambda} = 0. \tag{15}$$

Together with $\eta(0) = \eta_0$, this differential equation defines an initial value problem which, by numerical integration from $\lambda = 0$ to $\lambda = 1$, yields the desired solution $\eta(1)$ (see [11] for further details). As indicated by (15), the solution algorithm requires the computation of the Jacobian of $L(\alpha, \theta, \lambda)$, which is given by

$$\nabla L(\alpha, \theta, \lambda)^T = [L_\eta \quad L_\lambda] \tag{16}$$

where $L_\eta \triangleq \partial L/\partial\eta$ and $L_\lambda \triangleq \partial L/\partial\lambda$.

The expressions for these gradients are given in the Appendix. The combined prediction–correction sequence is presented in Table I. The algorithm starts with a correction step that updates the initial guess. When this step has converged, the value of λ is increased, and the changes in the multiplier coefficients are predicted in Step 3-d. The value of λ is increased until $||L(\alpha, \theta, \lambda)||$ is larger than a specified tolerance. The predictions of the coefficients η are then corrected in Step 4. The cycle is repeated until $\lambda = 1$ or the stability prediction limit is reached. The output from the program is a list of optimal multipliers and the cost overbound at several values of λ, which define the different guaranteed stability regions.

TABLE I
CONTINUATION ALGORITHM WHICH COMBINES PREDICTION TO NEW STABILITY BOUNDS AND CORRECTION OF THE MULTIPLIER COEFFICIENTS FOR GIVEN BOUNDS

Step 1. Initialize: loop = 0, $\Delta\lambda \in (0, 1]$ and determine appropriate values of α, N, and H for the compensator tested at M_{1o} and M_{2o}.

Step 2. Set loop = loop + 1. If loop = 1, then go to Step 4, else go to Step 3.

Step 3. Prediction:

- **a.** Set $\lambda_0 = \lambda$.
- **b.** Set $\lambda = \lambda_0 + \Delta\lambda$.
- **c.** Compute $\nabla L(\alpha, \theta, \lambda_0)$ and calculate $\eta'(\lambda_0)$ using

$$\eta'(\lambda_0) \triangleq \frac{d\eta}{d\lambda}\Big|_{\lambda=\lambda_0} = -[L_\eta(\alpha, \theta, \lambda_0)]^{-1} L_\lambda(\alpha, \theta, \lambda_0).$$

- **d.** Predict using $\eta(\lambda) = \eta(\lambda_0) + \Delta\lambda\,\eta'(\lambda_0)$.
- **e.** If $\|L(\alpha, \theta, \lambda)\| < \text{Tol}_1$, some pre-arranged tolerance (typically 1×10^{-5}), continue, else, reduce $\Delta\lambda$ and return to Step 3b.

Step 4. Correction:

- **a.** For current values of λ and η, compute $L(\alpha, \theta, \lambda)$ and L_η.
- **b.** Update $\eta(\lambda)$ using

$$\eta(\lambda) \leftarrow \eta(\lambda) - [L_\eta(\alpha, \theta, \lambda)]^{-1} L(\alpha, \theta, \lambda).$$

- **c.** If $\|L(\alpha, \theta, \lambda)\| < \text{Tol}_2$, some pre-arranged tolerance (typically $1\times10^2 \cdot \text{Tol}_1$), continue, else, reduce $\Delta\lambda$ and return to Step 4a.
- **d.** If $P(\lambda)$ is not nonnegative definite, STOP, else continue.
- **e.** Compute $\overline{J}$.
- **f.** If $\lambda < 1$, go to Step 2, else STOP.

The procedure in Table I is initialized by finding a set of scaling parameters for a given controller so that acceptable solutions exist for (7) and (9). Several algorithms, such as mixed $\mathcal{H}_2/\mathcal{H}_\infty$ [15] and μ with constant D-scales [16], can be used to develop initial values for H with $N = 0$. Note that the initialization problem is greatly simplified if the magnitudes of M_{1o} and M_{2o} are small and the compensators are robust in the sense that they have been desensitized to parameter variations. In this case, the controllers typically satisfy (7) and (9) for many different values of η. When one of these values of η is found, the first step of the algorithm determines values that optimize the cost overbound at the initial values of M_{1o} and M_{2o}. Determining more sophisticated techniques for developing initial conditions for this and other nonlinear optimization problems is the subject of current research.

III. ROBUST PERFORMANCE EXAMPLE

As an example of an application of this algorithm, we consider the robust performance analysis using several controllers that have been designed for the MACE. The code for the algorithms in the previous section were developed without special assumptions on the structure of the uncertainty model, but to be consistent with the previously presented synthesis algorithms, the following example considers the special case $C_0B_0 = 0$.

The experiment is a space shuttle flight project designed to demonstrate high authority active structural control in zero-gravity conditions. The MACE test article was configured to represent a precision-controlled, high payload mass fraction spacecraft, such as earth observing platforms, with multiple, independently pointing or scanning payloads. Thus the test article consists of a flexible bus to which are mounted two payloads, a reaction wheel assembly for attitude control, and

various other sensors and actuators. The goal of the active control is to maintain pointing accuracy of one payload, while the second payload is moving independently (see figure and discussion in [10] and [17]).

Controllers can be developed prior to flight using analytic finite element predictions of the test article dynamics. A key difficulty, however, is that the finite element models tend to be much less accurate than equivalently sized measurement models [18]. In particular, there tend to be substantial errors in some modal frequencies and damping ratios, even for the models of the ground-based test article. Since these FEM's are relatively inaccurate, they must be updated using measured data. In the MACE program these updates are done to the physical parameters of the system (i.e., the input to the analytic modeling technique) rather than modal parameters (i.e., the output), because the same physical parameters can then be used as the inputs for the 0–g model. Even with refinements made to the physical parameters, the 1–g model still exhibits significant discrepancies when compared to the measured data [8].

A variety of control experiments have been performed for the full XYZ dynamics of MACE. For this note, however, we consider a simpler control topology that only uses the dynamics about the X-axis. A white noise disturbance is applied to the secondary gimbal motor, and the actuator is the primary gimbal motor. The sensor and performance outputs are the X-axis payload inertial angular rate and angle, respectively, which are measured using the primary rate gyro. The nominal dynamics of a 37th-order design model from the MACE finite element model are written as

$$\begin{aligned} \dot{x} &= A_{ol}x + B_w w + B_u u, \\ z &= C_z x + D_{zu} u, \\ y &= C_y x + D_{yw} w + D_{yu} u \end{aligned} \tag{17}$$

where w is the disturbance to the secondary gimbal, u is the actuator command to the primary gimbal, z is the vector of performance variables (payload inertial angle as measured by the payload rate gyro and control effort), and y is the sensor measurement from the payload rate gyro. As discussed at length in [10] and [17], robust dynamic controllers $G_c(s)$ have been designed to minimize the $\mathcal{H}_2$ (quadratic) norm of the closed-loop transfer function from the disturbances to the performance variables. If we assume that the cross weighting matrices in the performance metric are all zero, the expected cost can be written as

$$J = \lim_{t\to\infty} \mathbb{E}\left\{z(t)^T R_{zz} z(t) + u(t)^T R_{uu} u(t)\right\} \tag{18}$$

subject to process noise with covariance V_{xx} and sensor noise with covariance V_{yy}. As usual, the values of $R_{uu} = \rho I$ and $V_{yy} = \mu I$ are used as design parameters to trade-off control authority (or performance) for robustness (or sensitivity). For simplicity in the following, we include all performance weights and noise intensities into the appropriate input or output matrices. The dynamic compensators are represented by

$$\dot{x}_c = A_c x_c + B_c y, \quad u = C_c x_c \tag{19}$$

TABLE II
FREQUENCY ERRORS FOR THE THREE MOST IMPORTANT MODES

Description	Measurement Model Frequency (Hz)	Finite Element Model Frequency (Hz)	errors (%)
1st Violin	7.21	6.84	-5.1
3rd Y bending	17.06	18.73	9.8
3rd Violin	21.54	20.67	-4.0

yielding the nominal closed-loop dynamics

$$\dot{\tilde{x}} = A_{cl}\tilde{x} + B_{cl} w, \quad z = C_{cl}\tilde{x} \tag{20}$$

where

$$\begin{aligned} \tilde{x} &\triangleq \begin{bmatrix} x \\ x_c \end{bmatrix}, \\ A_{cl} &\triangleq \begin{bmatrix} A_{ol} & B_u C_c \\ B_c C_y & A_c + B_c D_{yu} C_c \end{bmatrix}, \\ B_{cl} &\triangleq \begin{bmatrix} B_w \\ B_c D_{yw} \end{bmatrix}, \\ C_{cl} &\triangleq [C_z \quad D_{zu} C_c]. \end{aligned} \tag{21}$$

For this closed-loop system, the design parameters of the cost function are given by the non-negative definite matrices $R_{xx} = C_{cl}^T C_{cl}$ and $V_{xx} = B_{cl} B_{cl}^T$. If the uncertainty in the open-loop system is represented by $A_{ol} + \Delta A_{ol}$, then the model error for the closed-loop system is written as

$$\Delta A_{cl} \triangleq \begin{bmatrix} \Delta A_{ol} & 0_{n\times n_c} \\ 0_{n_c\times n} & 0_{n_c\times n_c} \end{bmatrix}. \tag{22}$$

The nominal system dynamics and model error in (20)–(22) can then be combined to write the actual closed-loop system dynamics in the form of (1).

Of course, for a system with many model errors, it is important to develop simple methods to determine which ones are most critical to the control design. For MACE, the primary error model is determined using both analysis techniques (such as the singular values of the sensitivity function and the multivariable Nichols test) evaluated on the model and the open-loop data, and preliminary, low-authority closed-loop experiments on the test article. For this FEM control design model, these techniques were used to determine that the frequencies of three modes were the most critical parameter errors. The errors in these three modes are listed in Table II. The finite element model results are compared with an identified model from measured data [18]. The "violin" description refers to modes with substantial interaction between the test article and the suspension system. Note that experience from these and other experiments has demonstrated that small errors in the damping values tend to degrade closed-loop performance, but small errors in the natural frequencies often lead to closed-loop instability. Thus, the model errors considered here address the more important issue of modal frequency uncertainty. For future comparison, note that the lowest frequency mode of these three was nearly destabilized by a very low-authority linear quadratic Gaussian (LQG) design that achieved only a 4 dB performance improvement.

Several robust control design techniques have been used in this work, and more complete details are provided in [2] and [17] and the references therein. Of course, the optimal controller for the MACE problem statement, without robustness considerations, can be obtained using LQG. One of the simplest robust control techniques is the sensitivity weighted LQG (SWLQG) approach which desensitizes the compensator to variations in the uncertain parameters with little additional computational effort. The maximum entropy (ME) approach uses a multiplicative white noise model to capture the effects of the parameter uncertainty on the system. A multiple model (MM) technique was also used to design controllers to simultaneously stabilize a set of plants, and minimize the weighted average of the squared $\mathcal{H}_2$ norms of the resulting closed-loop systems. When the models are selected in a manner that is representative of the uncertainty in the system, this technique can yield controllers that are robust to these parametric variations. Note that the LQG and SWLQG approaches have closed-form solutions, but the last two techniques are more complicated because they require numerical optimization.

1) Analysis: For the analysis of the robust controllers with respect to frequency uncertainty, the complex poles of the system A_{ol} matrix in (17) are written in second-order canonical form: block-diagonal (A_i), $i = 1, \cdots, k$, where

$$A_i = \begin{bmatrix} 0 & 1 \\ -\omega_i^2 & -2\zeta_i\omega_i \end{bmatrix} \tag{23}$$

and k refers to the number of complex poles. To determine ΔA_{ol}, the uncertainty in the modal frequency is then approximated as $\omega_i^2(1+\delta_i)$, where $\delta_i \in \mathbb{R}$ is called the frequency perturbation factor. Ranges for each δ_i can then be selected from Table II and incorporated into M_{1i} and M_{2i} for the analysis tests. For each uncertain mode, the perturbation to the nominal dynamics can be written as $\hat{A}_i = A_i + \Delta A_i$, where

$$\Delta A_i = \delta_i B_{0i} C_{0i},$$
$$B_{0i} = \begin{bmatrix} 0 \\ -\omega_i \end{bmatrix}$$

and

$$C_{0i} = [\omega_i \quad 0], \quad i = 1, \cdots, 3. \tag{24}$$

The B_0 and C_0 matrices for the open-loop system are constructed from these two sets and then represent the structure of the uncertainty in an internal feedback model. These matrices are augmented with additional zeroes to compensate for the dynamics of the controller, and then used to represent the structure of the uncertainty in the closed-loop system ΔA_{cl}.

To avoid an over parameterization of the multipliers in η, the analysis for these controllers was performed with $\alpha = 1$ and all of the diagonal elements of N and H arbitrary (provided $H > 0$ and $N \geq 0$). As discussed earlier, by setting $M_{2o} = -M_{1o} = 1 \times 10^{-3}$ and $\lambda_0 = 0$, initial values of N and H could easily be found by trial and error because the controllers are quite robust. Symmetric robustness bounds were used in the analysis, so $M_{2f} = -M_{1f} = I_3$. For the algorithm in Table I, typical increments for λ during the prediction step were approximately 0.007–0.013.

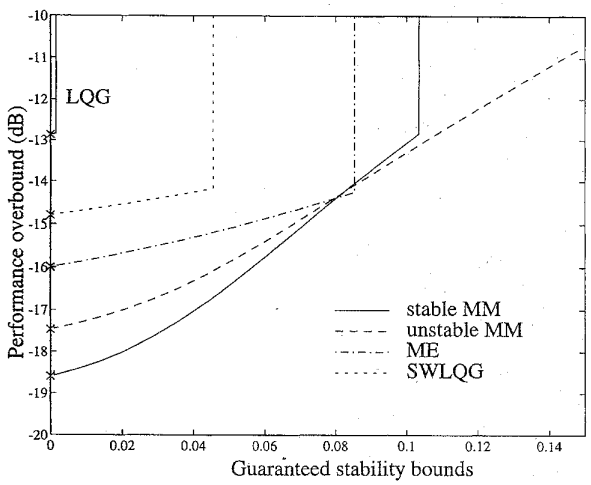

Fig. 1. Robust stability and performance analysis using several controllers for MACE. Symbols × indicate nominal $\mathcal{H}_2$ performance for each design.

The analysis results for the different controllers are compared in Fig. 1. Note that all of the compensators are unstable, except for the MM design that was constrained to be stable during the numerical optimization. Furthermore, all of the designs for this example are full order. The graph is a plot of performance improvement (in dB) versus the guaranteed stability bound $M_2(\lambda) = M_{2o} + \lambda(M_{2f} - M_{2o})$, $[M_1(\lambda) = -M_2(\lambda)]$. Recall that the performance corresponds to a reduction in the rms pointing angle error of the X-axis primary gimbal. The location of the vertical asymptotes in the curves corresponds to the limits of robust stability for that particular compensator. These analysis graphs differ from the ones in [10] which compare the optimal Popov controllers using the actual performance curves ("buckets") computed by perturbing the closed-loop dynamics.

For each controller, the symbol "×" on the performance axis indicates the $\mathcal{H}_2$ performance achieved by that design on the nominal design model. The SWLQG, ME, and MM designs represent the best performance that could be experimentally achieved using that particular technique. The techniques experimentally achieved 15 dB (SWLQG), 15.8 dB(ME), 20.2 dB (unstable MM compensator), and 19.7 dB (stable MM compensator) reductions in the regulation error component of the performance objective [17]. The best stabilizing LQG design was limited to approximately 4 dB performance on the hardware, so the LQG example in the figure is only presented to show the extreme sensitivity of the optimal controllers to changes in the modal frequencies.

The analysis results in Fig. 1 show the benefits of the different synthesis techniques. The SWLQG controller achieves reasonable performance and stability bounds given the relatively low computational effort required [17]. In comparison, the ME approach increases the robust stability region and yields better robust performance. These results are consistent with the better uncertainty model that is used in the approach. The stable MM design achieves the best robust performance of the controllers considered. The results also indicate that this design has a guaranteed robust stability limit greater than 10%

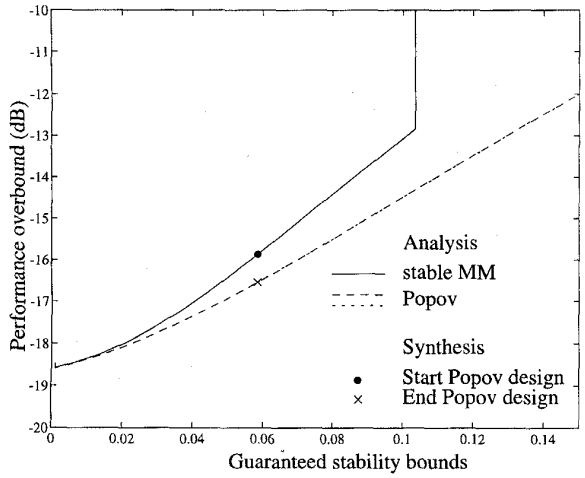

Fig. 2. Robust stability and performance improvements achieved by redesigning the controller using Popov controller synthesis. The two analysis curves for the Popov design show the insensitivity of the analysis technique to the initial starting point.

(i.e., approximately 5% in ω_i which is the anticipated error in two of the uncertain modes). As shown in the figure, there is a trade-off with the unstable MM controller between the nominal performance and larger robust stability bounds. The results of this analysis provide a good basis for comparing the control design approaches in terms of stability robustness and performance robustness. A comparison of the experimental performances achieved and the performance reductions predicted for large values of the guaranteed stability bounds (i.e., approximately 10%), however, provides an indication of the potential conservatism associated with obtaining guaranteed robust performance bounds via Popov analysis with symmetric bounds.

2) Synthesis: The results of this analysis can also be used to initialize a redesign of the robust controllers using Popov controller synthesis [5], [9]. An example of this procedure is illustrated in Fig. 2. The stable MM controller was used as the initial design, along with the multipliers computed at $M_2(\lambda) = 0.0585$. This point is indicated by the symbol "•" in Fig. 2. The controller was redesigned using a synthesis technique that optimizes the cost overbound with respect to both the multiplier coefficients and the controller gains. The synthesis optimization and stopping criterion are similar to the correction step in the analysis algorithm. In Fig. 2, the synthesis corresponds to a reduction in the cost overbound at a constant value of $M_2(\lambda)$. The final result is shown in the figure by the symbol "×" at $M_2(\lambda) = 0.0585$. As indicated, the robust performance at this level of the guaranteed stability bounds has been improved by almost 1 dB.

To complete this example, the new Popov design was then analyzed in two different ways. The algorithm was started at $\lambda_0 = 1 \times 10^{-3}$ with the same initial values used in the original MM analysis. The algorithm was also started using the multiplier values calculated by the synthesis code. These two analysis curves are essentially identical which shows that the analysis procedure is not overly sensitive to the initial conditions. These analysis results indicate that the Popov design achieves superior nominal and robust performance as compared to the MM controller, and that the robust stability boundaries are substantially improved ($\sim$ 20%).

Thus, Fig. 1 illustrates the utility of this analysis tool in an iterative control design methodology based on several robustness techniques with differing capabilities and computational requirements. Furthermore, Fig. 2 demonstrates that the Popov analysis and synthesis techniques can be combined to overcome the difficulty of developing initial values for the stability multipliers at large guaranteed stability bounds.

IV. Conclusions

This paper extends earlier work on optimal Popov analysis by developing algorithms for systems with multiple uncertainties that have both upper and lower sector-bounds. A typical application of this procedure was demonstrated by analyzing several robust controllers for MACE. A comparison of the analysis with the experimentally achieved performance of these controllers indicates a potential conservatism in the Popov analysis based on symmetric bounds. The optimal analysis was also used to initialize the synthesis algorithm to design a new controller that yields robust $\mathcal{H}_2$ performance with larger robust stability guarantees.

Appendix
Jacobian Expressions

As discussed, solving the homotopy problem requires the computation of the Jacobian of the homotopy map. The first part of the Jacobian in (16) is given by the symmetric matrix

$$L_\eta = \begin{bmatrix} \dfrac{\partial H_1}{\partial \alpha} & \cdots & \dfrac{\partial H_1}{\partial N_{ij}} & \cdots & \dfrac{\partial H_1}{\partial H_{ij}} \\ \bullet & \cdots & \mathrm{vec}_N\left(\dfrac{\partial H_2}{\partial N_{ij}}\right) & \cdots & \mathrm{vec}_N\left(\dfrac{\partial H_2}{\partial H_{ij}}\right) \\ \bullet & \cdots & \bullet & \cdots & \mathrm{vec}_N\left(\dfrac{\partial H_3}{\partial H_{ij}}\right) \end{bmatrix} \tag{25}$$

where H_1, H_2, and H_3 are defined in (10)–(12). Note that only the free parameters of N and H are considered in the calculation of L_η. Also, the columns of L_η are arranged to be consistent with the result produced by the $\mathrm{vec}_N(\cdot)$ operator. Let $E_{ij} = e_i e_j^T$, where each element of the column e_i is zero, except for the ith term which is unity. In the following, the dimension of E_{ij} is the same as the dimension of H. For convenience, we first note that

$$\frac{\partial \overline{C}}{\partial N_{ij}} = E_{ij} C_0 A_m,$$

$$\frac{\partial \overline{C}}{\partial H_{ij}} = E_{ij} C_0, \tag{26}$$

$$\frac{\partial C_{ricc}}{\partial \theta_j} = \frac{\partial \overline{C}}{\partial \theta_j} - B_0^T \frac{\partial P}{\partial \theta_j}, \tag{27}$$

$$\frac{\partial A_1}{\partial \theta_j} = -B_0 \left(\frac{\partial R_0^{-1}}{\partial \theta_j} \overline{C} + R_0^{-1} \frac{\partial \overline{C}}{\partial \theta_j} \right), \tag{28}$$

$$\frac{\partial R_0^{-1}}{\partial N_{ij}} = -R_0^{-1} [E_{ij} C_0 B_0 + (E_{ij} C_0 B_0)^T] R_0^{-1}, \tag{29}$$

$$\frac{\partial R_0^{-1}}{\partial H_{ij}} = -R_0^{-1}\{E_{ij}(M_2-M_1)^{-1} + [E_{ij}(M_2-M_1)^{-1}]^T\}R_0^{-1}, \tag{30}$$

$$\frac{\partial \overline{C}^T R_0^{-1}\overline{C}}{\partial \theta_j} = \overline{C}^T \frac{\partial R_0^{-1}}{\partial \theta_j}\overline{C} + \overline{C}^T R_0^{-1}\frac{\partial \overline{C}}{\partial \theta_j} + \left(\overline{C}^T R_0^{-1}\frac{\partial \overline{C}}{\partial \theta_j}\right)^T \tag{31}$$

where, as before, θ_j refers to any free element of H or N. The gradient expressions, in turn, depend on the solutions to the equations

$$0 = A_2^T\frac{\partial P}{\partial \alpha} + \frac{\partial P}{\partial \alpha}A_2 + R_{xx}, \tag{32}$$

$$0 = A_2\frac{\partial Q}{\partial \alpha} + \frac{\partial Q}{\partial \alpha}A_2^T - \frac{1}{\alpha^2}V_{xx} + B_0R_0^{-1}B_0^T\frac{\partial P}{\partial \alpha}Q + \left(B_0R_0^{-1}B_0^T\frac{\partial P}{\partial \alpha}Q\right)^T, \tag{33}$$

$$0 = A_2^T\frac{\partial P}{\partial \theta_j} + \frac{\partial P}{\partial \theta_j}A_2 + \frac{\partial A_1}{\partial \theta_j}^T P + P\frac{\partial A_1}{\partial \theta_j} + PB_0\frac{\partial R_0^{-1}}{\partial \theta_j}B_0^TP + \frac{\partial \overline{C}^T R_0^{-1}\overline{C}}{\partial \theta_j}, \tag{34}$$

$$0 = A_2\frac{\partial Q}{\partial \theta_j} + \frac{\partial Q}{\partial \theta_j}A_2^T + \left\{\left[\frac{\partial A_1}{\partial \theta_j} + B_0\left(\frac{\partial R_0^{-1}}{\partial \theta_j}B_0^TP + R_0^{-1}B_0^T\frac{\partial P}{\partial \theta_j}\right)\right]Q\right\} + \left\{\left[\frac{\partial A_1}{\partial \theta_j} + B_0\left(\frac{\partial R_0^{-1}}{\partial \theta_j}B_0^TP + R_0^{-1}B_0^T\frac{\partial P}{\partial \theta_j}\right)\right]Q\right\}^T. \tag{35}$$

Next, using (26)–(31), the elements of L_η in (25) can be written as

$$\frac{\partial H_1}{\partial \alpha} = \operatorname{tr}\left[\frac{\partial Q}{\partial \alpha}R_{xx}\right] - \frac{1}{\alpha^2}\operatorname{tr}\left[\frac{\partial P}{\partial \alpha}V_{xx}\right] + \frac{2}{\alpha^2}\overline{J}, \tag{36}$$

$$\frac{\partial H_1}{\partial N_{ij}} = \operatorname{tr}\left[\frac{\partial Q}{\partial N_{ij}}R_{xx}\right] - \frac{1}{\alpha^2}\operatorname{tr}\left[\frac{\partial P}{\partial N_{ij}}V_{xx}\right] - \frac{1}{\alpha^2}[(M_2-M_1)^TC_0V_{xx}C_0^T]_{ij}, \tag{37}$$

$$\frac{\partial H_1}{\partial H_{ij}} = \operatorname{tr}\left[\frac{\partial Q}{\partial H_{ij}}R_{xx}\right] - \frac{1}{\alpha^2}\operatorname{tr}\left[\frac{\partial P}{\partial H_{ij}}V_{xx}\right], \tag{38}$$

$$\frac{\partial H_2}{\partial \theta_j} = 2\left\{\left(\frac{\partial R_0^{-1}}{\partial \theta_j}C_{ricc} + R_0^{-1}\frac{\partial C_{ricc}}{\partial \theta_j}\right)QA_2^T + R_0^{-1}C_{ricc}\left[\frac{\partial Q}{\partial \theta_j}A_2^T - Q\left(\frac{\partial C_{ricc}^T}{\partial \theta_j}R_0^{-1} + C_{ricc}^T\frac{\partial R_0^{-1}}{\partial \theta_j}\right)B_0^T\right]\right\}C_0^T, \tag{39}$$

$$\frac{\partial H_3}{\partial H_{ij}} = 2\left(\left(\frac{\partial R_0^{-1}}{\partial H_{ij}}C_{ricc} + R_0^{-1}\frac{\partial C_{ricc}}{\partial H_{ij}}\right)Q \cdot [C_0 - (M_2-M_1)^{-1}R_0^{-1}C_{ricc}]^T + R_0^{-1}C_{ricc} \cdot \left\{\frac{\partial Q}{\partial H_{ij}}[C_0 - (M_2-M_1)^{-1}R_0^{-1}C_{ricc}]^T - Q\left(\frac{\partial C_{ricc}^T}{\partial H_{ij}}R_0^{-1} + C_{ricc}^T\frac{\partial R_0^{-1}}{\partial H_{ij}}\right)\cdot (M_2-M_1)^{-1}\right\}\right) \tag{40}$$

where $[\cdot]_{ij}$ corresponds to the value in the ith row and jth column of the matrix. To perform the prediction, it is necessary to compute

$$L_\lambda = \left\{\left(\frac{\partial H_1}{\partial \lambda}\right)^T, \left[\operatorname{vec}_N\left(\frac{\partial H_2}{\partial \lambda}\right)\right]^T, \left[\operatorname{vec}_N\left(\frac{\partial H_3}{\partial \lambda}\right)\right]^T\right\}^T. \tag{41}$$

Again, we first note that

$$\frac{\partial \overline{C}}{\partial \lambda} = -NC_0B_0(M_{1f}-M_{1o})C_0, \tag{42}$$

$$\frac{\partial C_{ricc}}{\partial \lambda} = \frac{\partial \overline{C}}{\partial \lambda} - B_0^T\frac{\partial P}{\partial \lambda}, \tag{43}$$

$$\frac{\partial A_1}{\partial \lambda} = -B_0\left[(M_{1f}-M_{1o})C_0 + \frac{\partial R_0^{-1}}{\partial \lambda}\overline{C} + R_0^{-1}\frac{\partial \overline{C}}{\partial \lambda}\right], \tag{44}$$

$$\frac{\partial \overline{C}^T R_0^{-1}\overline{C}}{\partial \lambda} = \overline{C}^T\frac{\partial R_0^{-1}}{\partial \lambda}\overline{C} + \overline{C}^TR_0^{-1}\frac{\partial \overline{C}}{\partial \lambda} + \left(\overline{C}^TR_0^{-1}\frac{\partial \overline{C}}{\partial \lambda}\right)^T, \tag{45}$$

$$\frac{\partial R_0^{-1}}{\partial \lambda} = R_0^{-1}(\{H(M_2-M_1)^{-1}[(M_{2f}-M_{2o}) - (M_{1f}-M_{1o})](M_2-M_1)^{-1}\} + \{H(M_2-M_1)^{-1}[(M_{2f}-M_{2o}) - (M_{1f}-M_{1o})](M_2-M_1)^{-1}\}^T)R_0^{-1} \tag{46}$$

which are based on the solutions to the equations

$$0 = A_2^T\frac{\partial P}{\partial \lambda} + \frac{\partial P}{\partial \lambda}A_2 + \frac{\partial A_1}{\partial \lambda}^T P + P\frac{\partial A_1}{\partial \lambda} + PB_0\frac{\partial R_0^{-1}}{\partial \lambda}B_0^TP + \frac{\partial \overline{C}^TR_0^{-1}\overline{C}}{\partial \lambda}, \tag{47}$$

$$0 = A_2\frac{\partial Q}{\partial \lambda} + \frac{\partial Q}{\partial \lambda}A_2^T + \left\{\left[\frac{\partial A_1}{\partial \lambda} + B_0\left(\frac{\partial R_0^{-1}}{\partial \lambda}B_0^TP + R_0^{-1}B_0^T\frac{\partial P}{\partial \lambda}\right)\right]Q\right\} + \left\{\left[\frac{\partial A_1}{\partial \lambda} + B_0\left(\frac{\partial R_0^{-1}}{\partial \lambda}B_0^TP + R_0^{-1}B_0^T\frac{\partial P}{\partial \lambda}\right)\right]Q\right\}^T. \tag{48}$$

Then L_λ in (41) can be written in terms of

$$\frac{\partial H_1}{\partial \lambda} = \operatorname{tr}\left[\frac{\partial Q}{\partial \lambda}R_{xx}\right] - \frac{1}{\alpha^2}\operatorname{tr}\left(\left\{\frac{\partial P}{\partial \lambda} + C_0^T \cdot [(M_{2f}-M_{2o}) - (M_{1f}-M_{1o})]NC_0\right\}V_{xx}\right), \tag{49}$$

$$\frac{\partial H_2}{\partial \lambda} = \frac{1}{\alpha}\left[(M_{2f}-M_{2o})-(M_{1f}-M_{1o})\right]^T C_0 V_{xx} C_0^T + 2\left[\left(\frac{\partial R_0^{-1}}{\partial \lambda} C_{ricc} + R_0^{-1}\frac{\partial C_{ricc}}{\partial \lambda}\right) Q A_2^T + R_0^{-1} C_{ricc}\left\{\frac{\partial Q}{\partial \lambda} A_2^T - Q\left[\frac{\partial C_{ricc}^T}{\partial \lambda} R_0^{-1} + C_{ricc}^T \frac{\partial R_0^{-1}}{\partial \lambda} + C_0^T (M_{1f}-M_{1o})\right] B_0^T\right\}\right] C_0^T, \quad (50)$$

$$\frac{\partial H_3}{\partial \lambda} = 2\left\{\left(\frac{\partial R_0^{-1}}{\partial \lambda} C_{ricc} + R_0^{-1}\frac{\partial C_{ricc}}{\partial \lambda}\right) Q \cdot [C_0-(M_2-M_1)^{-1}R_0^{-1}C_{ricc}]^T + R_0^{-1}C_{ricc}\left\{\frac{\partial Q}{\partial \lambda}[C_0-(M_2-M_1)^{-1}R_0^{-1}C_{ricc}]^T - Q\left\{\frac{\partial C_{ricc}^T}{\partial \lambda} R_0^{-1} + C_{ricc}^T\left[\frac{\partial R_0^{-1}}{\partial \lambda} - R_0^{-1}(M_2-M_1)^{-1} \cdot [(M_{2f}-M_{2o})-(M_{1f}-M_{1o})]\right]\right\} \cdot (M_2-M_1)^{-1}\right\}\right\}. \quad (51)$$

Note that each of the Lyapunov equations for the derivative terms has the same dynamics matrix, A_2. In this work, the Lyapunov equations are solved using an eigenvalue decomposition of A_2. Thus, the decomposition need only be performed once per Hessian calculation, which significantly decreases the computational effort required to determine this matrix.

ACKNOWLEDGMENT

The authors would like to thank the MACE team at MIT (especially R. Glaese, S. Grocott, and Dr. D. Miller).

REFERENCES

[1] J. P. How, R. M. Glaese, S. C. O. Grocott, and D. W. Miller, "Finite element model based robust controllers for the MIT Middeck active control experiment (MACE)," in *Proc. Amer. Contr. Conf.*, Piscataway, NJ, June 1994, pp. 272–277.

[2] S. C. O. Grocott, J. P. How, D. W. Miller, D. G. MacMartin, and K. Liu, "Robust control design and implementation on the Middeck active control experiment (MACE)," *AIAA J. Guid., Contr., Dynamics*, vol. 17, pp. 1163–1170, Nov./Dec. 1994.

[3] V. M. Popov, "On absolute stability of nonlinear automatic control systems," *Avtomat. Telemekh.*, vol. 22, no. 8, pp. 961–979, 1961.

[4] K. S. Narendra and J. H. Taylor, *Frequency Domain Criteria for Absolute Stability*. New York: Academic, 1973.

[5] J. P. How, "Robust control design with real parameter uncertainty using absolute stability theory," Ph.D. dissertation, Dep. Aeronautics Astronautics, Massachusetts Inst. Technol., Cambridge, MA, MIT SERC Rep. 1-93, Feb. 1993.

[6] W. M. Haddad and D. S. Bernstein, "Parameter-dependent Lyapunov functions and the Popov criterion in robust analysis and synthesis," *IEEE Trans. Automat. Contr.*, vol. 40, pp. 536–543, Mar. 1994.

[7] E. G. Collins, Jr., W. M. Haddad, and L. D. Davis, "Riccati equation approaches for robust stability and performance analysis using the small gain, positivity, and Popov theorems," *AIAA J. Guidance., Contr., Dynamics*, pp. 322–329, June 1994.

[8] R. Glaese and D. W. Miller, "On-orbit modeling of the Middeck active control experiment from 1-g analysis and experimentation," in *Proc. 12th Int. Modal Anal. Conf. (IMAC)*, Feb. 1994, pp. 1107–1113.

[9] J. P. How, W. M. Haddad, and S. R. Hall, "Application of Popov controller synthesis to benchmark problems with real parameter uncertainty," *AIAA J. Guidance, Contr., Dynamics*, vol. 17, pp. 759–768, July/Aug. 1994.

[10] J. P. How, S. R. Hall, and W. M. Haddad, "Robust controllers for the Middeck active control experiment using Popov controller synthesis," *IEEE Trans. Contr. Syst. Technol.*, vol. 2, pp. 73–87, June 1994.

[11] E. G. Collins, Jr., L. D. Davis, and S. Richter, "Design of reduced-order, $\mathcal{H}_2$ optimal controllers using a homotopy algorithm," *Int. J. Contr.*, vol. 61, pp. 97–126, 1995.

[12] W. M. Haddad and D. S. Bernstein, "Parameter-dependent Lyapunov functions, constant real parameter uncertainty, and the Popov criterion in robust analysis and synthesis, Parts I and II," in *Proc. IEEE Conf. Decision Contr.*, Dec. 1991, pp. 2274–2279, 2632–2633.

[13] S. L. Richter and R. A. DeCarlo, "Continuation methods: Theory and applications," *IEEE Trans. Automat. Contr.*, vol. AC-30, pp. 347–352, 1983.

[14] L. T. Watson, "Numerical linear algebra aspects of globally convergent homotopy methods," *SIAM Rev.*, pp. 529–545, 1986.

[15] D. S. Bernstein and W. M. Haddad, "LQG control with an $\mathcal{H}_\infty$ performance bound: A Riccati equation approach," *IEEE Trans. Automat. Contr.*, vol. 34, pp. 293–305, Mar. 1989.

[16] W. M. Haddad, E. G. Collins, Jr., and R. Moser, "Fixed structure computation of the structured singular value," in *Proc. Amer. Contr. Conf.*, Piscataway, NJ, June 1993, pp. 1673–1674.

[17] S. C. O. Grocott, J. P. How, and D. W. Miller, "Comparison of robust control techniques for uncertain structural systems," in *AIAA Guidance, Navigation, Contr. Conf.*, Aug. 1994, pp. 261–271, submitted to the *AIAA J. Guidance, Contr., Dynamics.*

[18] K. Liu and D. W. Miller, "System identification by the ORSE technique with a finite number of data samples," in *Proc. Amer. Contr. Conf.*, Piscataway, NJ, June 1993, pp. 2310–2315.